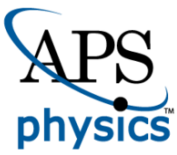

This is the accepted manuscript made available via CHORUS. The article has been published as:

Photoinduced Nonequilibrium Topological States in Strained Black Phosphorus

Hang Liu, Jia-Tao Sun, Cai Cheng, Feng Liu, and Sheng Meng

Phys. Rev. Lett. **120**, 237403 — Published 8 June 2018

DOI: 10.1103/PhysRevLett.120.237403

Photoinduced nonequilibrium topological states in strained black phosphorus

Hang Liu,[1,4] Jia-Tao Sun,[1,4,*] Cai Cheng,[1] Feng Liu,[2,3,†] and Sheng Meng[1,3,4,‡]

[1] *Institute of Physics, Chinese Academy of Sciences, Beijing 100190, P. R. China*

[2] *Department of Materials Science and Engineering, University of Utah, Salt Lake City, Utah 84112, USA*

[3] *Collaborative Innovation Center of Quantum Matter, Beijing 100084, P. R. China*

[4] *University of Chinese Academy of Sciences, Beijing 100049, P. R. China*

Black phosphorus (BP), an elemental semiconductor, has attracted tremendous interest because it exhibits a wealth of interesting electronic and optoelectronic properties in equilibrium condition. The nonequilibrium electronic structures of bulk BP under a periodic field of laser remain unexplored, but can lead to intriguing topological optoelectronic properties. Here we show that under the irradiation of circularly polarized light (CPL) BP exhibits photo-dressed Floquet Dirac semimetal state, which can be continuously tuned by changing the direction, intensity and frequency of incident laser. The topological phase transition from type-I to type-II Floquet-Dirac fermions manifests a new form of type-III phase which exists in a wide range of intensity and frequency of incident laser. Furthermore, topological surface states exhibit nonequilibrium electron transport in a direction locked by the helicity of CPL. Our findings not only deepen our understanding of fundamental properties of BP in relation to topology but also extend optoelectronic device applications of BP to nonequilibrium regime.

Since the experimental exfoliation of single-layer graphene [1-3], layered elemental materials like silicene, germanene and stanene [4-8] continue to emerge enabling outstanding electronic and optoelectronic properties for applications in nanoscale devices. Black phosphorous (BP) is a new member of layered elemental materials gaining renewed attention, thanks to its remarkable anisotropic optical [9], electrical [10,11], excitonic [9,12], thermal properties [13] and their accessible control by strain *etc* [14]. Unlike others like graphene and stanene, which are intrinsic topological materials, BP in ambient condition is topological trivial. The topologically nontrivial type-I Dirac state can exist conditionally depending on thickness [15], carrier doping [16], and electric field [17-20] endowing BP with feasible control on charge carriers. Nevertheless other topological states such as type-II Dirac state violating the relativistic Lorentz invariance has not been found so far [21]. The phase boundary between type-I and type-II states (Fig. 1) would be critical for the applications of BP in exotic optoelectronics since it allows unidirectional quantum transport [22,23]. Given all the interesting equilibrium electronic/optoelectronic properties and exotic optoelectronic applications envisioned, the topological phase transition (TPT) in BP deserves much attention.

Recently optical pumping of solids has been shown to offer new possibilities for exploring novel states of matter absent in equilibrium systems [24,25]. In particular, quantum phase transitions between the photon-dressed states (Floquet-Bloch states) can facilitate nonequilibrium quantum transport to be driven by a laser. A number of nonequilibrium photon-dressed phases with topologically protected edge state have been theoretically proposed by periodic monochromatic pumping on an ultrafast time-scale [24-33]. However, experimental evidences to confirm photoinduced topological sates and phase transitions remain to be explored, because real material systems which can realize these theoretical models are rare [24,25,34]. Moreover, model calculations can hardly map the whole Brillouin zone of solids, especially when the band manifolds are complex and entangled.

In this Letter we studied compressively strained BP under a periodic field of circularly polarized laser (CPL) based on the Floquet theorem where the band manifolds were obtained by first-principles calculation in the framework of density functional theory and then fit with

Wannier functions. We propose that it offers an appealing material platform to explore the photoinduced topological states and their TPTs. Quantum phase transitions between type-I and type-II Floquet-Dirac fermions (FDFs) can be achieved by tuning the direction, intensity, and frequency of incident CPL, originated from optical Stark effect. Moreover, the type-III FDF with a Dirac line Fermi surface is identified. Furthermore, the electron transport direction of surface states is shown to be locked with the helicity of CPL, enabling feasible control of quantum transport in BP by optical means. Our work extends the potential applications of BP to nonequilibrium regime.

Bulk BP with AB stacking order is an elemental layered semiconductor with a narrow direct band gap of 0.33 ± 0.02 eV [35,36], located at the time-reversal invariant momentum Z (Fig. S1) [37]. The top of valence band and the bottom of conduction band possess an even (+) and odd (−) parity, respectively [51]. Our calculation shows that, upon applying a 2% uniaxial compressive strain along the armchair direction, the direct band gap decreases to zero resulting in an anisotropic Dirac semimetal. Further compression leads to crossing of valence and conduction bands and inverted band parities, forming a type-I Dirac nodal ring lying in the Γ-Z-W plane (Fig. 1 and Fig. S1), which has been studied by previous calculations and experiments [52-54]. On the contrary, tensile strain increases band gap, which cannot form desired Dirac ring electronic state [14]. For the convenience of calculations, we select compressive strain of 3.72% in this work which is larger than 2%.

To study coherent interactions between a laser and strained BP, we adopt an anticlockwise CPL with a time-dependent vector potential $\boldsymbol{A}(t) = A_0(\cos(\omega t), \sin(\omega t), 0)$ (see Supplemental Material [37] for details). The time-periodic and space-homogeneous CPL propagates along the stacking direction ($-z$) of BP (Fig. 2(a)). The photon energy and amplitude of the CPL are set as $\hbar\omega$ = 0.5 eV and A_0 = 150 V/c (corresponding to 0.038 V/Å or 1.9×10^{10} W/cm^2, here c is velocity of light), respectively. For a laser pulse with a brief duration of 6 cycles (long enough to realize Floquet states [55]), the laser fluence is only 1‰ of the threshold to break BP [56], suggesting the energy deposition and heating effect is small [34,57,58]. We find that the Dirac nodal ring in equilibrium is simultaneously driven to a pair of type-I Floquet-Dirac nodal points along the Γ-Z-Γ path, and topologically nontrivial gaps

emerge on other paths in the Γ-Z-W plane, as shown in Fig. 2(c,d). When the amplitude of CPL increases to A_0 = 300 V/c, type-I nodal points are taken over by type-II nodal points (Fig. 2(g,h)). At the same time, the separation between the pair of nodal points decreases from 0.142 Å^{-1} to 0.068 Å^{-1}. During the transitions between type-I and type-II states, a new Dirac state, called the type-III state with flat band of the cone, would appear (Fig. 2(e,f)). The type-III Dirac state is a new type of topological state, which can host new types of fermion quasiparticles. In the type-III Dirac materials, the Fermi surface is a Dirac line connected at the nodal point.

Evolution of Fermi surface contours of the irradiated BP with laser is shown in Fig. 1(f-i) and Fig. 2(d,f,h). When the Fermi level is at the energy of type-II nodal points $\varepsilon_F = \varepsilon_D$, the electron and hole pockets coexists for photoinduced type-II FDF (Fig. 2(j)), which differs from the type-I nodal point induced by CPL with weak amplitude. When ε_F is at the energy of $\varepsilon_D \pm 1.5$ meV, the electron and hole pockets stay away from each other (Fig. 2(i,k)). Moreover, the Dirac line Fermi surface of type-III state enters between Fermi surfaces of type-I FDF and type-II FDF (Fig. 2(f)). The special Fermi surfaces of both type-II and type-III FDFs promises the extraordinary transport properties [59,60].

The TPT shown above depends not only on the laser amplitude, but also on the incident direction of CPL. For example, if the incident direction of CPL is along the zigzag (y) direction, one can obtain type-I nodal points and topologically trivial bandgap in turn with the increasing laser amplitude, while type-III and type-II nodal points are absent (Fig. S2) [37]. This angular dependence of Floquet states originates from anisotropic atomic structure of BP, which suggests that topological Floquet states can be easily engineered by tuning the incident direction and amplitude of laser.

To study the continuous evolution of TPTs, the phase diagram as functions of laser intensity and incident direction is constructed, as shown in Fig. 3(c). The angle-resolved and time-dependent vector potential $\boldsymbol{A}(t) = A_0(\cos(\omega t), \sin(\omega t)\sin(\theta), \sin(\omega t)\cos(\theta))$ with fixed photon energy $\hbar\omega$ = 0.5 eV is used, where θ is the angle between the propagation direction of CPL (red arrow) and zigzag (y) direction (Fig. 3(a)). Emergence of type-I FDFs has a weak

dependence on the incident direction. In contrast, type-III and type-II FDFs have a strong dependence on the incident direction, and can be obtained with moderate laser intensity. When the propagation direction of CPL deviates from the high-symmetry paths ($\theta \neq 0°, 90°$), nodal points do not appear along the laser propagation direction, but develop an orientation mismatch ($\theta' \neq \theta$) (see Fig. S3 for details [37]). Here θ' represents the angle of the line connecting two laser-induced nodal points with respect to k_y axis (or Z-W path).

Besides the incident direction and amplitude of CPL, the photon energy of CPL is another degree of freedom to engineer the TPT from type-I to type-II FDFs. Figure 3(d) shows the phase diagram when the incident direction of CPL is restricted to align with the stacking direction ($\theta = 90°$). We find that the states with type-I FDFs exist in a large range of photon energy and laser amplitude. In contrast, type-II FDFs can only be induced by the CPL with moderate amplitude and infrared photon energy. Consequently, the following conditions to realize TPT from type-I to type-II FDFs are required simultaneously: i) Light propagation is restricted along the stacking direction ($\theta = 70° \sim 90°$); ii) Laser amplitude and photon energy are set in the ranges of $A_0 = 150 \sim 350$ V/c and $\hbar\omega = 0.2 \sim 1.0$ eV.

Next, to reveal the mechanism of above TPTs, we consider the case of CPL with a vector potential $\boldsymbol{A}(t) = A_0(\cos(\omega t), \sin(\omega t), 0)$ propagating along the stacking direction of BP. Once the CPL is irradiated on BP, the electrons would emit and absorb photons to form photon-dressed (or side) bands labelled by Floquet band index $n = \cdots, -2, -1, 1, 2, \cdots$ (gray thin line in Fig. 4(a)), while the static component is indexed with $n = 0$ (gray bold line in Fig. 4(a)). The photon-dressed states would hybridize with $n = 0$ states, known as optical Stark effect, leading to band repulsion $\Delta = \sqrt{A_0^2 |M|^2 + (\delta E)^2} - \delta E$ [55]. Here M is the dipole matrix element between the two states, and δE is the energy difference of the two states before hybridization. Because the energy difference between $n = 0$ and $n = -1$ bands is zero ($\delta E = 0$) at their crossing points, the induced gap Δ increases linearly with laser amplitude A_0.

The energy difference between the original nodal point in equilibrium and the crossing point of $n = 0$ and $n = -1$ bands on the Γ-Z path is defined as Δ' (Fig. 4(a)). Obviously, in order to drive the TPT from type-I to type-II FDFs, the optical Stark effect should be strong

enough to satisfy $\Delta/2 > \Delta'$. When photon energy is fixed to $\hbar\omega = 0.5$ eV, the energy difference Δ' is 0.17 eV (pink dashed line in Fig. 4(c)). The crossing point (type-III state) of the pink dashed line and pink solid line separates type-II (above pink dashed line) from type-I Floquet-Dirac states (below pink dashed line). However, when photon energy increases sufficiently (e.g. $\hbar\omega$ = 1.5 eV), the energy difference Δ' can be so large that the requirement $\Delta/2 > \Delta'$ cannot be satisfied before the two type-I nodal points merge together (Fig. 4(b)). Consequently, the type-III and type-II FDFs can no longer be realized. Furthermore, as shown in Fig. 4(d), the phase boundary (type-III FDF) between type-I and type-II FDFs can be plotted according to the crossing points of dashed and solid lines in Fig. 4(c). It is seen that the phase boundary results from the linear dependence of $\Delta \sim A_0$ and the linear dispersions around the nodal point. Besides the crucial role of optical Stark effect played in the TPT from type-I to type-II FDFs, the weak dependence of shift of nodal points on photon energy, as shown in Fig. 4(b), is also contributed by this effect, which is missing in previous model Hamiltonian calculations [49].

In equilibrium, the strained BP has a drumhead surface state in the surface Brillouin zone (SBZ) of the (100) surface (Fig. S1) [52]. It is natural to ask if nonequilibrium surface states protected from backscattering also appear in the strained BP under light irradiation. When turning on CPL to propagate along the stacking direction ($-z$), the strained BP has the nodal points along Γ-Z-Γ path and topologically nontrivial gaps along other paths (Γ-Z-W plane) (see Fig. 2(c)). The Floquet surface states along $\bar{\Gamma}$-$\bar{Z}$-$\bar{\Gamma}$ path connect two nodal points (Fig. S4) [37], while along other paths on SBZ passing $\bar{Z}$, surface states connect two topologically nontrivial gaps of type-I FDFs. Along $\bar{W}$-$\bar{Z}$-$\bar{W}$ (or $\bar{k}_y$) direction, the surface states of type-I FDFs at two opposite surfaces have opposite slopes (Fig. 5(a-c)). Two Fermi arcs contributed by two opposite surfaces connect two nodal points (Fig. S4) [37].

As sketched in Fig. 5(a-c), if the helicity of CPL is set to be counterclockwise, the transport directions of nonequilibrium surface states on left (right) surface are along $+y$ ($-y$). Once the helicity of CPL is changed to be clockwise, the direction of topologically protected transport channel on each surface would be reversed (Fig. 5(d-f)). The locking effect is independent of the type of FDFs (Fig. S5) [37]. Therefore, by changing CPL frequency and

amplitude, not only the dispersions of surface states can be tuned, but also the Fermi arc of the FDFs. If the laser incident direction is along other paths in the Γ-Z-W plane, the locking effect of the transport direction with respect to the laser helicity remains valid (Fig. S6) [37]. The robust locking for the topological Floquet-Dirac states provides an effective method to control the dissipationless surface states by laser illumination.

In conclusion, a number of nonequilibrium topological phases in the uniaxially compressed BP under the irradiation of CPL have been identified, including various types of FDFs and Floquet topological insulators. The TPTs between them can be engineered by tuning incident direction, intensity and photon energy of the CPL. The intriguing TPT from type-I to type-II FDFs is predicted when infrared laser with moderate strength propagates along the stacking direction of BP. The transport directions of novel nonequilibrium surface states, resulted from bulk-boundary correspondence of the topological Floquet-Dirac states, are locked with the helicity of CPL, providing the possibility to optically control nonequilibrium quantum transport properties. Therefore, our findings deepen our fundamental understanding of optoelectronic properties of BP in relation to topology and extend optoelectronic device applications of BP to nonequilibrium regime. Besides, the type-III Floquet-Dirac fermions are promising for realizing the solid-state analogue of Hawking radiation [61,62].

We gratefully acknowledge financial support from the National Key R&D Program of China (Grant No. 2016YFA0202300, 2016YFA0300902, 2015CB921001), National Basic Research Program of China (Grant No. 2013CBA01600), and "Strategic Priority Research Program (B)" of Chinese Academy of Sciences (Grant No. XDB07030100). F. L. was supported by US DOE-BES (No. DE-FG02-04ER46148).

* jtsun@iphy.ac.cn
† fliu@eng.utah.edu
‡ smeng@iphy.ac.cn

[1] K. S. Novoselov, A. K. Geim, S. V. Morozov, D. Jiang, Y. Zhang, S. V. Dubonos, I. V. Grigorieva, and A. A. Firsov, Science **306**, 666 (2004).

[2] A. H. Castro Neto, F. Guinea, N. M. R. Peres, K. S. Novoselov, and A. K. Geim, Rev. Mod. Phys. **81**, 109 (2009).

[3] K. S. Novoselov, Z. Jiang, Y. Zhang, S. V. Morozov, H. L. Stormer, U. Zeitler, J. C. Maan, G. S. Boebinger, P. Kim, and A. K. Geim, Science **315**, 1379 (2007).
[4] S. Cahangirov, M. Topsakal, E. Aktürk, H. Şahin, and S. Ciraci, Phys. Rev. Lett. **102**, 236804 (2009).
[5] P. Vogt, P. De Padova, C. Quaresima, J. Avila, E. Frantzeskakis, M. C. Asensio, A. Resta, B. n. d. Ealet, and G. Le Lay, Phys. Rev. Lett. **108**, 155501 (2012).
[6] M. Houssa, G. Pourtois, V. V. Afanas'ev, and A. Stesmans, Appl. Phys. Lett. **96**, 082111 (2010).
[7] F.-f. Zhu, W.-j. Chen, Y. Xu, C.-l. Gao, D.-d. Guan, C.-h. Liu, D. Qian, S.-C. Zhang, and J.-f. Jia, Nat. Mater. **14**, 1020 (2015).
[8] A. Molle, J. Goldberger, M. Houssa, Y. Xu, S.-C. Zhang, and D. Akinwande, Nat. Mater. **16**, 163 (2017).
[9] X. Wang, A. M. Jones, K. L. Seyler, V. Tran, Y. Jia, H. Zhao, H. Wang, L. Yang, X. Xu, and F. Xia, Nat. Nanotech. **10**, 517 (2015).
[10] F. Xia, H. Wang, and Y. Jia, Nat. Commun. **5**, 4458 (2014).
[11] X. Ling, H. Wang, S. X. Huang, F. N. Xia, and M. S. Dresselhaus, Proc. Natl. Acad. Sci. U. S. A. **112**, 4523 (2015).
[12] V. Tran, R. Soklaski, Y. F. Liang, and L. Yang, Phys. Rev. B **89**, 6, 235319 (2014).
[13] Z. Luo, J. Maassen, Y. Deng, Y. Du, R. P. Garrelts, M. S. Lundstrom, P. D. Ye, and X. Xu, Nat. Commun. **6**, 8572 (2015).
[14] G. Zhang, S. Huang, A. Chaves, C. Song, V. O. Ozcelik, T. Low, and H. Yan, Nat. Commun. **8**, 14071 (2017).
[15] J. Qiao, X. Kong, Z.-X. Hu, F. Yang, and W. Ji, Nat. Commun. **5**, 4475 (2014).
[16] J. Kim, S. S. Baik, S. H. Ryu, Y. Sohn, S. Park, B. G. Park, J. Denlinger, Y. Yi, H. J. Choi, and K. S. Kim, Science **349**, 723 (2015).
[17] B. Deng, V. Tran, Y. Xie, H. Jiang, C. Li, Q. Guo, X. Wang, H. Tian, S. J. Koester, H. Wang, J. J. Cha, Q. Xia, L. Yang, and F. Xia, Nat. Commun. **8**, 14474 (2017).
[18] L. Li, Y. Yu, G. J. Ye, Q. Ge, X. Ou, H. Wu, D. Feng, X. H. Chen, and Y. Zhang, Nat. Nanotech. **9**, 372 (2014).
[19] Q. Liu, X. Zhang, L. B. Abdalla, A. Fazzio, and A. Zunger, Nano Lett. **15**, 1222 (2015).
[20] J. Kim, S. S. Baik, S. W. Jung, Y. Sohn, S. H. Ryu, H. J. Choi, B.-J. Yang, and K. S. Kim, Phys. Rev. Lett. **119**, 226801 (2017).
[21] K. Deng, G. Wan, P. Deng, K. Zhang, S. Ding, E. Wang, M. Yan, H. Huang, H. Zhang, Z. Xu, J. Denlinger, A. Fedorov, H. Yang, W. Duan, H. Yao, Y. Wu, S. Fan, H. Zhang, X. Chen, and S. Zhou, Nat. Phys. **12**, 1105 (2016).
[22] M. Buscema, D. J. Groenendijk, S. I. Blanter, G. A. Steele, H. S. J. van der Zant, and A. Castellanos-Gomez, Nano Lett. **14**, 3347 (2014).
[23] A. Castellanos-Gomez, J. Phys. Chem. Lett. **6**, 4280 (2015).
[24] E. J. Sie, J. W. McIver, Y. H. Lee, L. Fu, J. Kong, and N. Gedik, Nat. Mater. **14**, 290 (2015).
[25] Y. H. Wang, H. Steinberg, P. Jarillo-Herrero, and N. Gedik, Science **342**, 453 (2013).
[26] M. A. Sentef, M. Claassen, A. F. Kemper, B. Moritz, T. Oka, J. K. Freericks, and T. P. Devereaux, Nat. Commun. **6**, 7047 (2015).
[27] A. G. Grushin, A. Gomez-Leon, and T. Neupert, Phys. Rev. Lett. **112**, 156801 (2014).
[28] L. D'Alessio and M. Rigol, Nat. Commun. **6**, 8336 (2015).
[29] N. H. Lindner, G. Refael, and V. Galitski, Nat. Phys. **7**, 490 (2011).
[30] M. C. Rechtsman, J. M. Zeuner, Y. Plotnik, Y. Lumer, D. Podolsky, F. Dreisow, S. Nolte, M. Segev, and A. Szameit, Nature **496**, 196 (2013).

[31] A. A. Reynoso and D. Frustaglia, Phys. Rev. B **87**, 115420 (2013).
[32] F. Wilczek, Phys. Rev. Lett. **109**, 160401 (2012).
[33] D. V. Else, B. Bauer, and C. Nayak, Phys. Rev. Lett. **117**, 090402 (2016).
[34] E. J. Sie, C. H. Lui, Y.-H. Lee, L. Fu, J. Kong, and N. Gedik, Science **355**, 1066 (2017).
[35] M. Batmunkh, M. Bat-Erdene, and J. G. Shapter, Adv. Mater. **28**, 8586 (2016).
[36] R. W. Keyes, Phys. Rev. **92**, 580 (1953).
[37] See Supplemental Material at http://link.aps.org/supplemental/xxx, for details about the calculation methods, atomic structure, other photoinduced states and corresponding surface states, which includes Refs. [38-50].
[38] G. Kresse and J. Furthmuller, Phys. Rev. B **54**, 11169 (1996).
[39] J. P. Perdew, K. Burke, and M. Ernzerhof, Phys. Rev. Lett. **77**, 3865 (1996).
[40] A. A. Mostofi, J. R. Yates, Y. S. Lee, I. Souza, D. Vanderbilt, and N. Marzari, Comput. Phys. Commun. **178**, 685 (2008).
[41] A. A. Mostofi, J. R. Yates, G. Pizzi, Y.-S. Lee, I. Souza, D. Vanderbilt, and N. Marzari, Comput. Phys. Commun. **185**, 2309 (2014).
[42] N. Marzari, A. A. Mostofi, J. R. Yates, I. Souza, and D. Vanderbilt, Rev. Mod. Phys. **84**, 1419 (2012).
[43] J. H. Shirley, Phys. Rev. **138**, B979 (1965).
[44] H. Sambe, Phys. Rev. A **7**, 2203 (1973).
[45] K. F. Milfeld and R. E. Wyatt, Phys. Rev. A **27**, 72 (1983).
[46] M. P. L. Sancho, J. M. L. Sancho, and J. Rubio, Journal of Physics F: Metal Physics **15**, 851 (1985).
[47] M. P. L. Sancho, J. M. L. Sancho, and J. Rubio, Journal of Physics F: Metal Physics **14**, 1205 (1984).
[48] T. Bzdusek, Q. Wu, A. Ruegg, M. Sigrist, and A. A. Soluyanov, Nature **538**, 75 (2016).
[49] Z. Yan and Z. Wang, Phys. Rev. Lett. **117**, 087402 (2016).
[50] R. Wang, B. Wang, R. Shen, L. Sheng, and D. Y. Xing, EPL (Europhysics Letters) **105**, 17004 (2014).
[51] H. Asahina and A. Morita, J. Phys. C: Solid State Phys. **17**, 1839 (1984).
[52] J. Zhao, R. Yu, H. Weng, and Z. Fang, Phys. Rev. B **94**, 195104 (2016).
[53] Z. J. Xiang, Phys. Rev. Lett. **115**, 186403 (2015).
[54] C.-H. Li, Y.-J. Long, L.-X. Zhao, L. Shan, Z.-A. Ren, J.-Z. Zhao, H.-M. Weng, X. Dai, Z. Fang, C. Ren, and G.-F. Chen, Phys. Rev. B **95**, 125417 (2017).
[55] U. De Giovannini, H. Hubener, and A. Rubio, Nano Lett. **16**, 7993 (2016).
[56] G. Qiu, Q. Nian, M. Motlag, S. Jin, B. Deng, Y. Deng, A. R. Charnas, P. D. Ye, and G. J. Cheng, Adv. Mater. **30**, 1704405 (2018).
[57] S. K. Sundaram and E. Mazur, Nat. Mater. **1**, 217 (2002).
[58] F. Mahmood, C.-K. Chan, Z. Alpichshev, D. Gardner, Y. Lee, P. A. Lee, and N. Gedik, Nat. Phys. **12**, 306 (2016).
[59] A. A. Soluyanov, D. Gresch, Z. Wang, Q. Wu, M. Troyer, X. Dai, and B. A. Bernevig, Nature **527**, 495 (2015).
[60] Z. M. Yu, Y. Yao, and S. A. Yang, Phys. Rev. Lett. **117**, 077202 (2016).
[61] G. E. Volovik and K. Zhang, J. Low Temp. Phys. **189**, 276 (2017).
[62] H. Huang, K.-H. Jin, and F. Liu, arXiv: 1711.07096.

Figures:

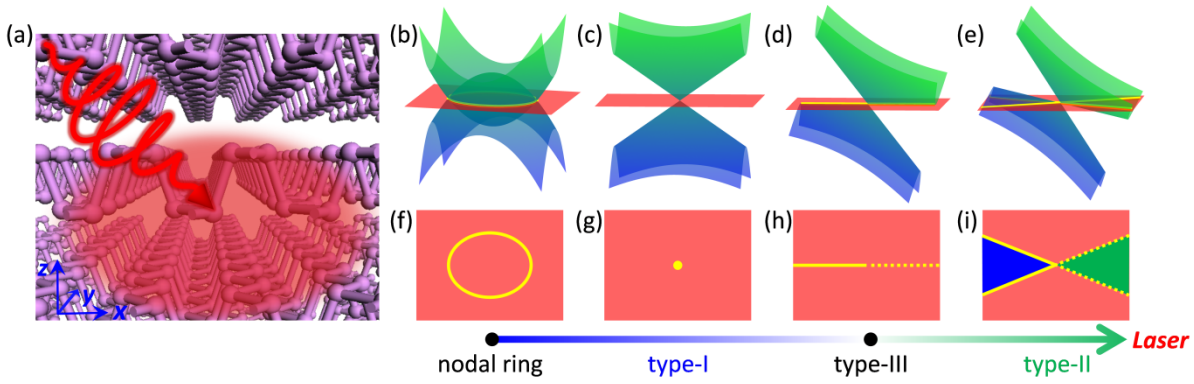

FIG. 1. (Color online) (a) Schematic illustration of compressed BP irradiated by CPL. The *x*, *y* and *z* axes are along armchair, zigzag and stacking directions respectively. (b-e) Laser-driven phase transitions from Dirac nodal ring to type-I, type-III and type-II Dirac points in BP. (f-i) Evolution of Fermi surface with CPL.

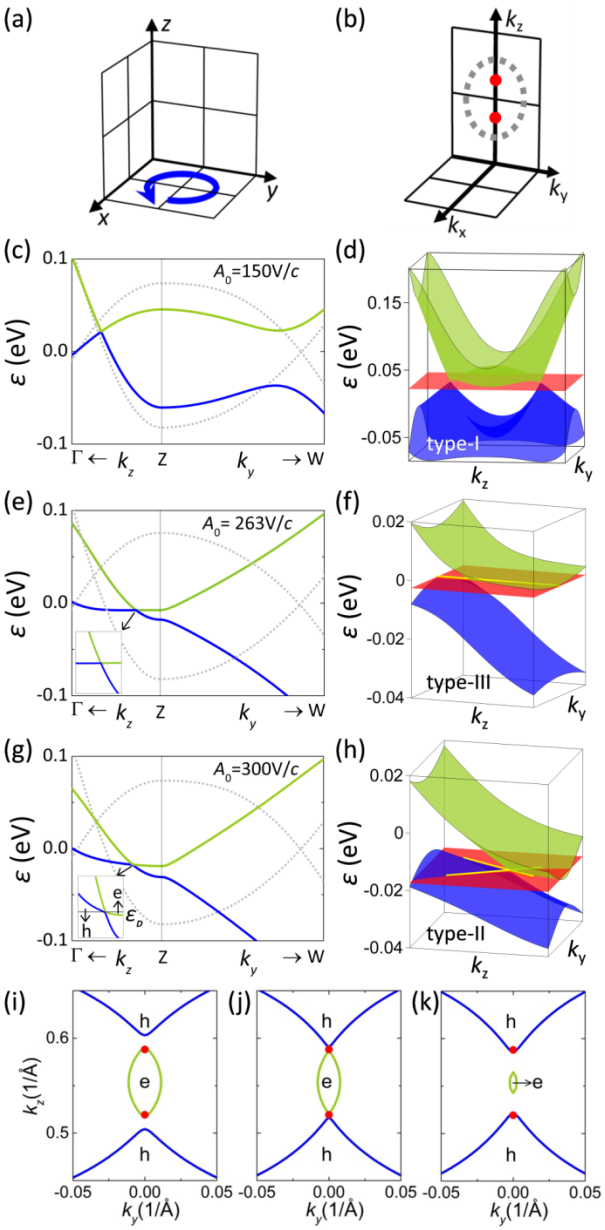

FIG. 2. (Color online) Topological FDFs induced by laser with photon energy $\hbar\omega$ = 0.5 eV. (a) CPL $\boldsymbol{A}(t) = A_0(\cos(\omega t),\sin(\omega t),0)$ propagates along stacking direction ($-z$). (b) The laser-induced Floquet-Dirac nodal points (red points) and original nodal ring in equilibrium (dashed circle). Floquet-Bloch band structure and band diagram of BP driven by laser with amplitude A_0 = 150 V/c (c,d), A_0 = 263 V/c (e,f) and A_0 = 300 V/c (g,h). Gray dotted line is the equilibrium electronic structure. The quasienergy of nodal points is marked as ε_D. Yellow lines on red plane represent Fermi surfaces. (i-k) Fermi contour lines on the k_x = 0 (Γ-Z-W) plane when Fermi energy is at ε_D + 1.5 meV, ε_D, ε_D − 1.5 meV respectively. The red dots are the positions of projected type-II nodal points on k_x = 0 plane. The green closed ellipses and blue open hyperbolas represent the contours of the electron and hole pockets in the plane k_x = 0 respectively.

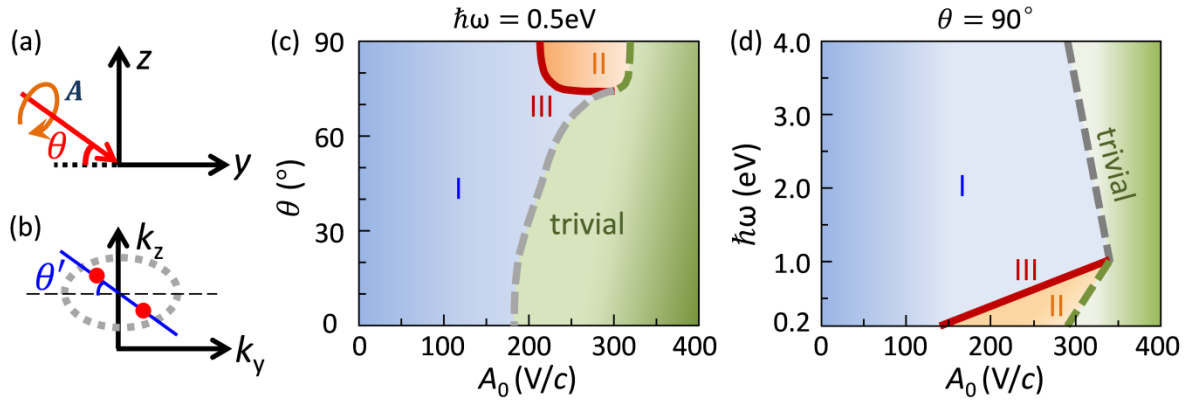

FIG. 3. (Color online) Laser-induced Floquet phase diagram of compressively strained BP. (a) Anticlockwise CPL propagates on the *yz* plane with the propagation direction as θ. (b) The gray circle represents equilibrium nodal ring of strained BP. The angle between connecting line of two Floquet-Dirac nodal points (red dots) and k_y direction is θ'. (c) Phase diagram of laser-driven BP (photon energy $\hbar\omega$ = 0.5 eV) on the dependence of laser amplitude A_0 and incident angle θ. (d) The Floquet phases induced by laser (θ = 90°) with different amplitude A_0 and frequency ω.

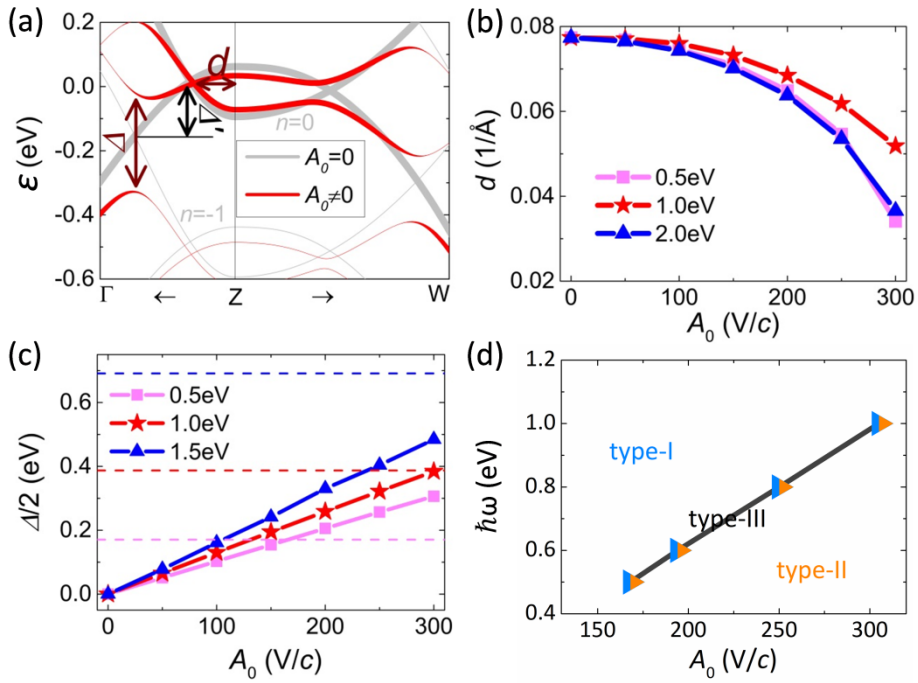

FIG. 4. (Color online) Origin of the Floquet phase transition of BP driven by CPL propagating along stacking direction ($-z$). (a) The bold and thin gray lines represent $n = 0$ and $n = -1$ Floquet-Bloch bands respectively. Δ' is the energy difference between Dirac point on nodal ring and the crossing of $n = 0$ and $n = -1$ bands along Γ-Z direction. The thickness of the line is proportional to the weight of the static ($n = 0$) component . Band gap Δ is induced by the hybridization between bands indexed by $n = 0$ and $n = -1$. The distance between Floquet-Dirac nodal point and center of the nodal ring is marked as d. (b) The variation of d with laser amplitude A_0 when the photon energy is set as $\hbar\omega = 0.5$, 1.0 and 2.0 eV respectively. (c) The dependence of $\Delta/2$ on laser amplitude A_0 when photon energy is set as $\hbar\omega = 0.5$, 1.0 and 1.5 eV respectively. Dashed lines represent the value Δ' in three cases. (d) Linear dependence of the photon energy and laser amplitude defining the phase boundary of type-I and type-II Floquet-Dirac phases.

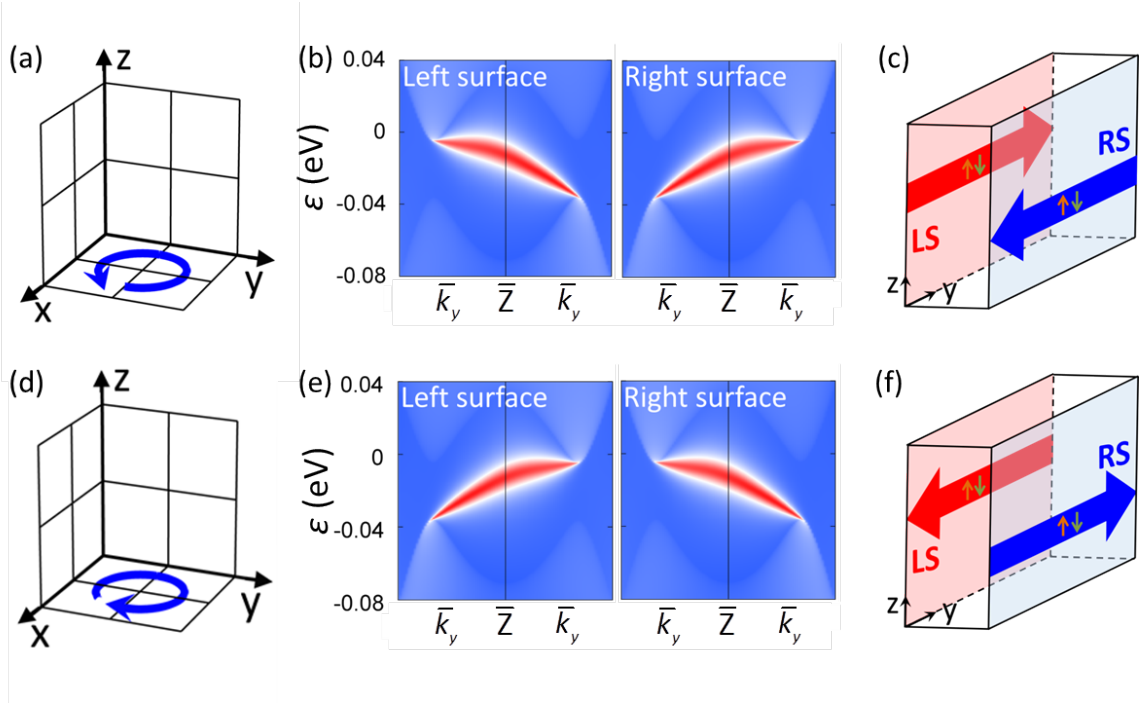

FIG. 5. (Color online) The locking effect of the transport direction of surface states and laser helicity. (a) The sketch of laser helicity. (b) Surface states along $\bar{W}$-$\bar{Z}$-$\bar{W}$ direction in SBZ come from left and right surfaces respectively, which is induced by laser with photon energy $\hbar\omega$ = 0.9 eV and amplitude A_0 = 150 V/c. (c) The opposite direction of topologically protected surface currents on two counter surfaces. LS: left surface; RS: right surface. (d-f) Surface states of Floquet-Dirac state when the laser helicity is reversed.